Supporting Information

Correlation between Structural Features and Activity Trend of Fe Surfaces for Ammonia Synthesis

Jianfu Chen[a1], Ye Chen[a1], Haifeng Wang[a] and P. Hu[b,c,*]

[a] State Key Laboratory of Green Chemical Engineering and Industrial Catalysis, Key Laboratory for Advanced Materials, Centre for Computational Chemistry and Research Institute of Industrial Catalysis, East China University of Science and Technology, 130 Meilong Road, Shanghai 200237, China
[b] School of Physical Science and Technology, ShanghaiTech University, 393 Middle Huaxia Road, Shanghai 201210, China
[c] School of Chemistry and Chemical Engineering, The Queen's University of Belfast, Belfast BT9 5AG, United Kingdom
[1] The authors contributed equally to this work

Corresponding Author

*E-mail address: p.hu@qub.ac.uk

S1. Surface model and computational details

A *p*(3x3) supercell was constructed to calculate the elementary reactions of ammonia synthesis on various Fe surfaces. As is shown in **Fig. S1**, the layer number varies; there are 6 layers for Fe(100), 5 layers for Fe(110), 4 layers for Fe(111), Fe(210) and Fe(211), respectively. When optimizing the structure for each elementary reaction, the top 2~3 layers with the surface species were fully relaxed while the rest of bottom layers of the surface model were fixed. A 15 Å vacuum region was placed on the top of the model.

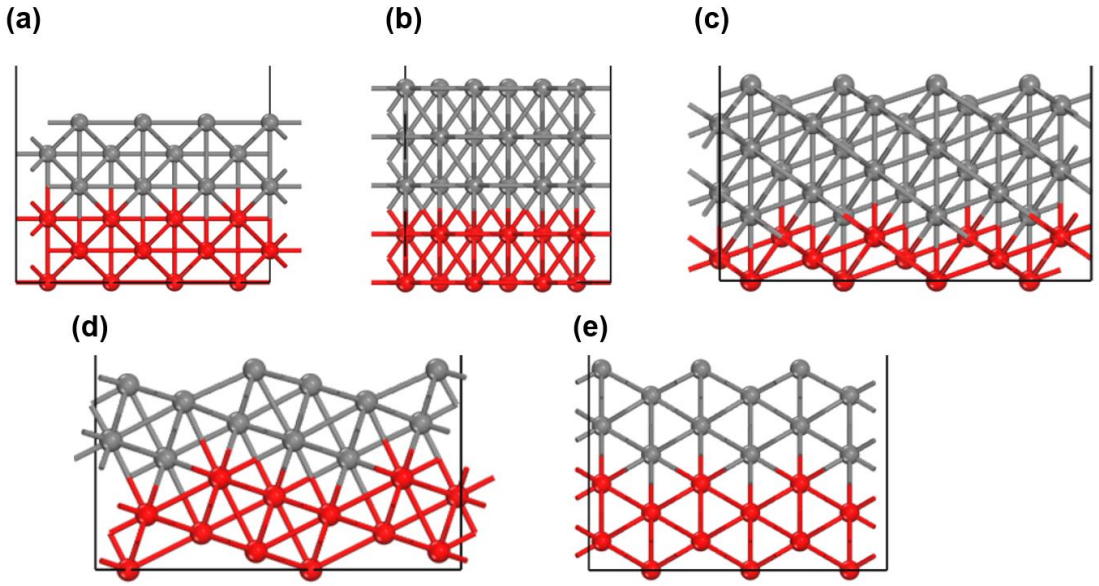

Fig. S1 Side views of *p*(3×3) Fe surfaces. (a) Fe(100) (96 atoms, 11.336×11.336 $Å^2$). (b) Fe(110) (60 atoms, 8.016×8.502 $Å^2$). (c) Fe(111) (120 atoms, 12.023×13.883 $Å^2$). (d) Fe(210) (96 atoms, 11.336×12.674 $Å^2$) and (e) Fe(211) (120 atoms, 12.271×12.023 $Å^2$). The thicknesses of the employed slabs vary, with 7.085 Å for Fe(100), 8.016 Å for Fe(110), 7.363 Å for Fe(111), 6.971 Å for Fe(210), and 8.099 Å for Fe(211), respectively. Gray balls represent for relaxed atoms, while red balls represent for fixed atoms.

The convergence tests for k-point grids have been performed using the adsorption energy of N on Fe(111). Based on the consideration of the test results and computational cost, the surface Monkhorst Pack meshes of 2 × 2 × 1 k-point sampling in the surface Brillouin zone were used for the surfaces for both coverage-dependent and coverage-independent calculations.

Table S1. Surface energies (eV) and magnetic moment of various k-points on Fe(111) at a cut-off energy of 450 eV.

k-points	111	121	131	221	321	331	441
surf	-941.865	-941.400	-941.248	-940.985	-940.923	-940.869	-940.911
MAG	301.520	302.580	303.140	301.230	302.300	302.490	302.420
surf_N	-951.300	-950.788	-950.673	-950.398	-950.363	-950.315	-950.331
MAG	302.660	302.180	303.800	301.050	302.540	303.100	302.800
E_{ad}	-1.121	-1.074	-1.111	-1.099	-1.127	-1.132	-1.106

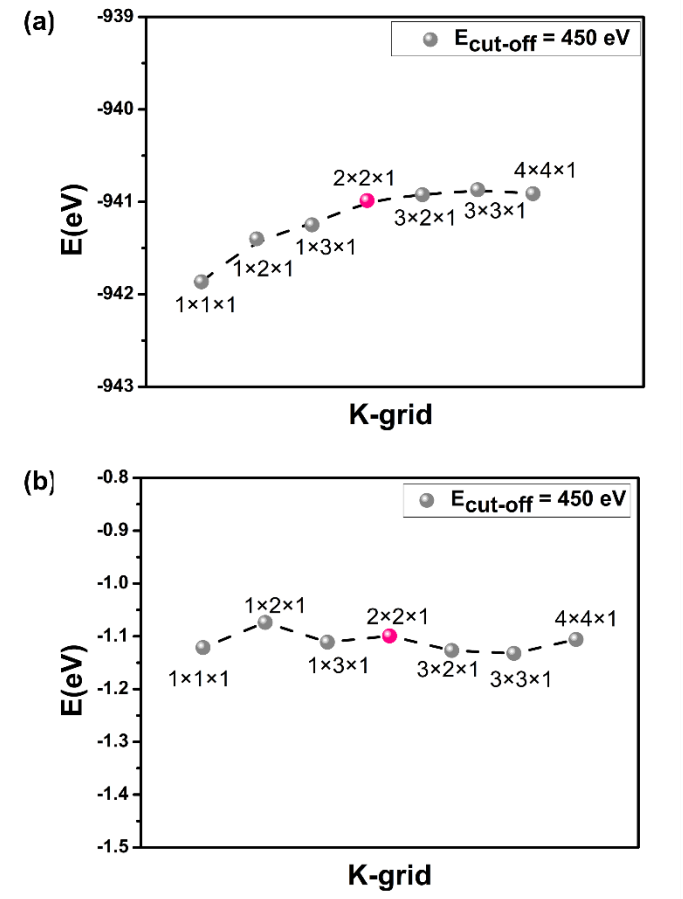

Fig. S2 At a cut-off energy of 450 eV, (a) the total energy of the Fe(111) surface changes with k-point sampling; and (b) the adsorption energy of a nitrogen atom on Fe(111) varies with k-point sampling.

S2. Elementary steps in coverage-dependent microkinetic modelling

To simplify the calculation, we combined the adsorption of N_2 and the dissociation of N_2* into one reaction step. Taking the most active Fe(111) surface as an example, the coverage-independent microkinetic modelling was performed to calculate the TOF based on DFT calculated, leading to a predicted TOF = 4.2 s^{-1} per site, being in the same order of magnitude with the original result of TOF = 2.6 s^{-1} per site. The steady-state intermediate distributions obtained was shown in **Fig. S3(b)**, which is in perfect accordance with the original distributions (**Fig. S3(a)**), indicating to be feasible. The elementary steps in coverage-dependent microkinetic modelling are listed in **Table S2**.

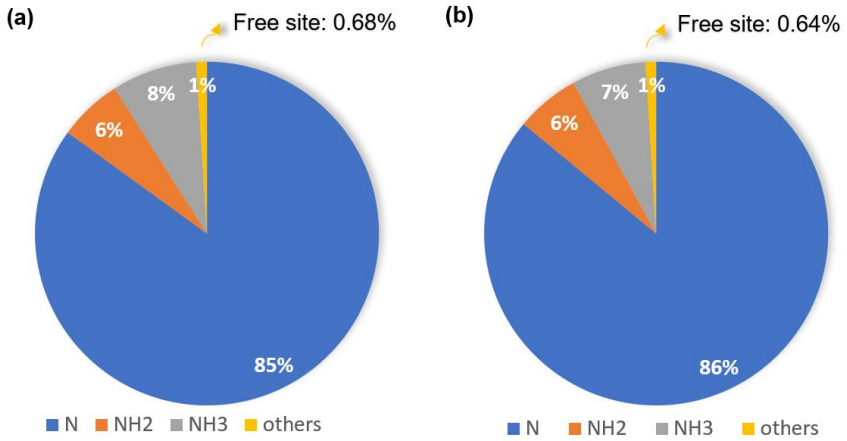

Fig. S3 Surface species distributions from microkinetic simulation results for NNR on Fe(111) using the coverage-independent model at 673 K and 20 bar (N_2: H_2: NH_3= 1:3:0.01, an experimental condition). (a) Coverage distribution results from microkinetic simulations for the elementary steps described in Table 1 in the main text; and (b) coverage distribution results obtained by combining the adsorption of N_2 and the dissociation of N_2* into one reaction step (see Table S2). Others include H, NH and free site.

Table S2 Elementary steps and the rate equations of ammonia synthesis used in the coverage-dependent microkinetic modelling (* represents the free site on the surface).

	Surface Reactions	Rate Equations
1	$H_2(g) + 2* \leftrightarrow 2H*$	$r_1 = k_1 P_{H_2} \theta_*^2 - k_{-1} \theta_H^2$
2	$N_2(g)+2* \leftrightarrow N*+N*$	$r_2 = k_2 P_{N_2} \theta_*^2 - k_{-2} \theta_N^2$
3	$N* + H* \leftrightarrow NH* + *$	$r_3 = k_3 \theta_N \theta_H - k_{-3} \theta_{NH} \theta_*$
4	$NH* + H* \leftrightarrow NH_2*+ *$	$r_4 = k_4 \theta_{NH} \theta_H - k_{-4} \theta_{NH_2} \theta_*$

5	$NH_2^* + H^* \leftrightarrow NH_3^* + *$	$r_5 = k_5\theta_{NH_2}\theta_H - k_{-5}\theta_{NH_3}\theta_*$
6	$NH_3^* \leftrightarrow NH_3 + *$	$r_6 = k_6\theta_{NH_3} - k_{-6}P_{NH_3}\theta_*$

S3. Adsorption structures of the coverage-dependent model

The most stable structure on the Fe(111) for each adsorption state was searched for all adsorbates including N*, NH*, NH_2*, NH_3* and H* with the consideration of both self- and cross-interactions. Based on the previous optimization of the adsorption structures of N, NH_2, NH_3, H and NH, it is evident that N and NH prefer hollow-site adsorption, H and NH_2 prefer bridge-site adsorption, while NH_3 favors top-site adsorption (**Fig. S4**). An example set of optimized structures of N*/$NH_{2(env)}$, NH*/$NH_{2(env)}$, NH_2*/$NH_{2(env)}$, NH_3*/$NH_{2(env)}$ and H*/$NH_{2(env)}$ are shown in **Fig. S5** to **S9**.

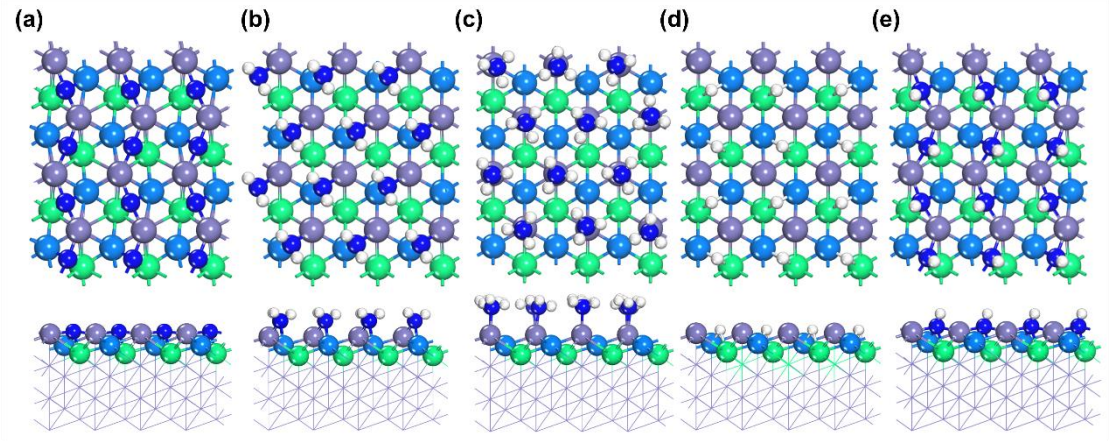

Fig. S4 At a coverage of 1 ML, environmental species exhibit the most stable structures for (a) N, (b) NH_2, (c) NH_3, (d) H and (e) NH, respectively. The Fe(111) surface consists of three layers; grey, blue and green balls indicate the top layer, the second layer and the third layer of Fe, respectively. Dark blue atoms represent N atoms and white atoms represent H atoms.

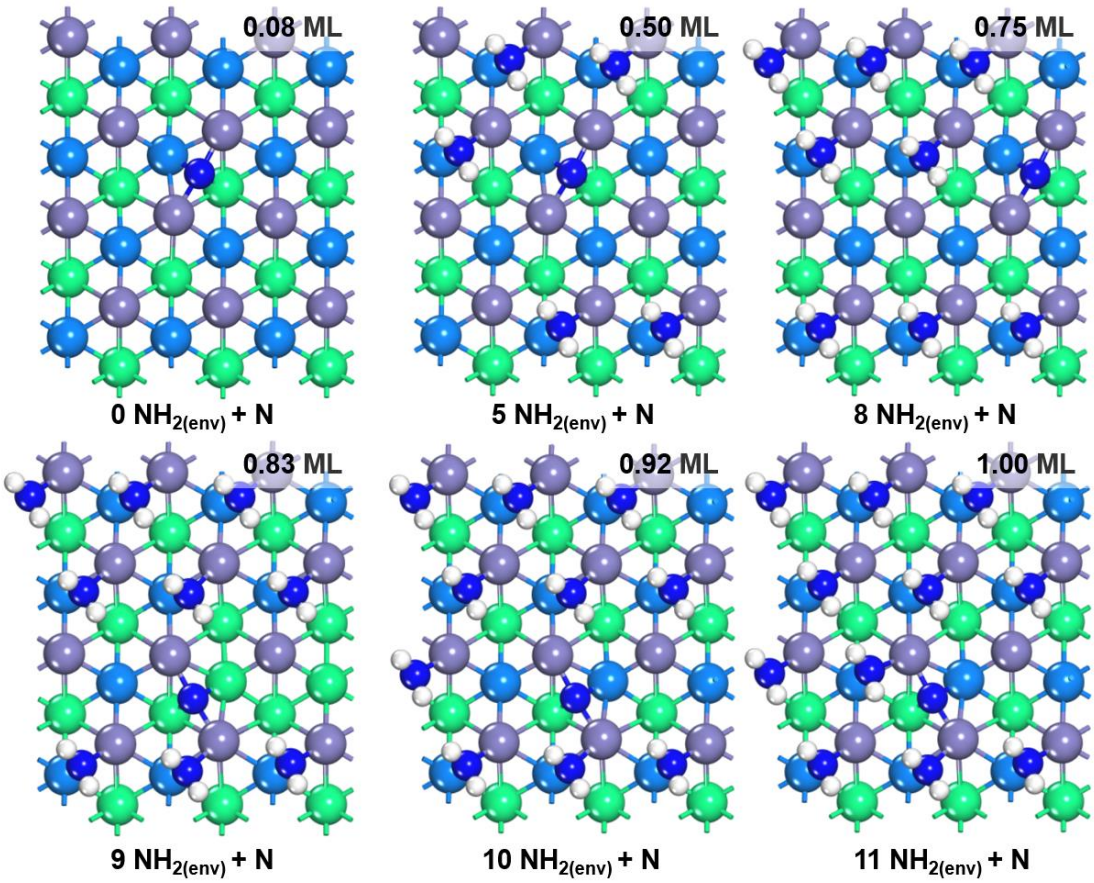

Fig. S5 Most stable structures of N*/$NH_{2(env)}$ on the Fe(111) surface at various corresponding coverages.

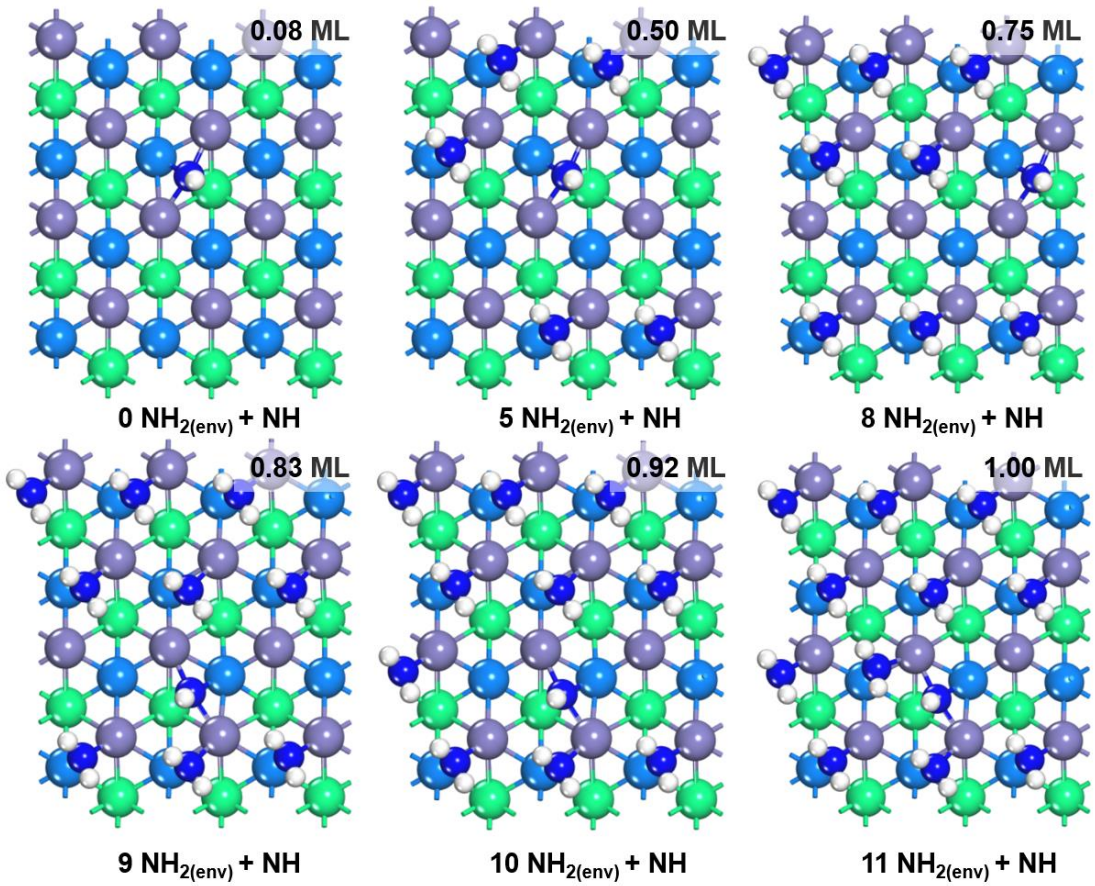

Fig. S6 Most stable structures of NH*/ $NH_{2(env)}$ on the Fe(111) surface at various corresponding coverages.

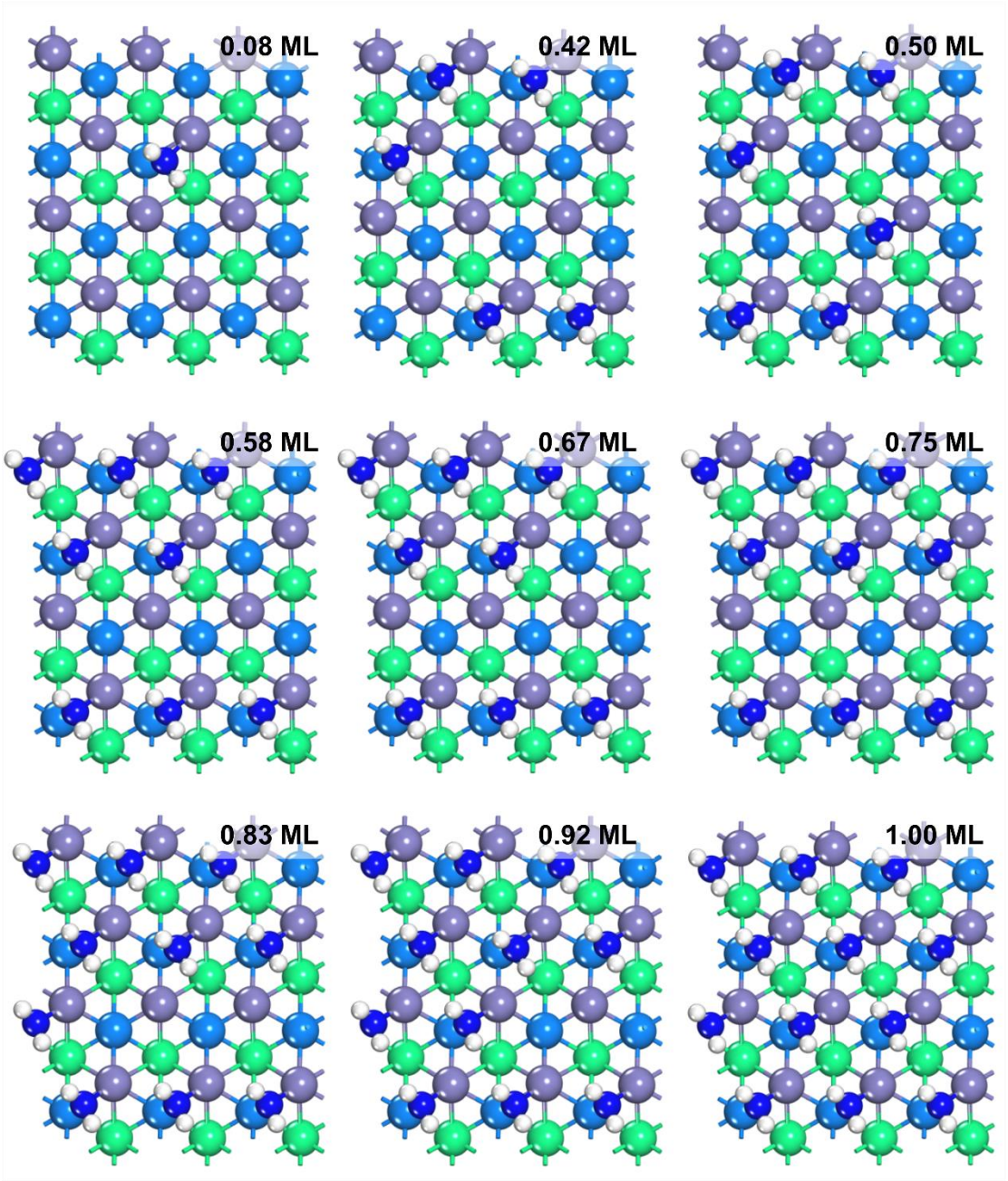

Fig. S7 Most stable structures of NH_2*/$NH_{2(env)}$ on the Fe(111) surface at various corresponding coverages.

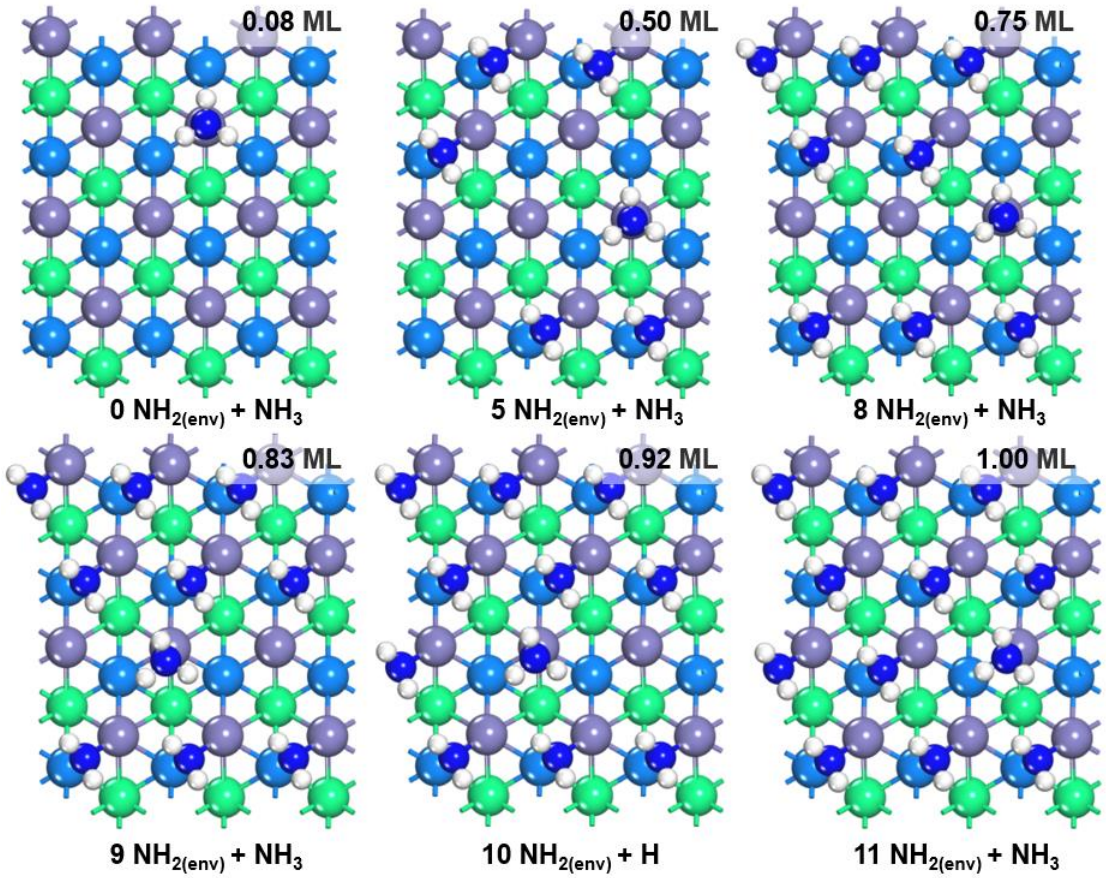

Fig. S8 Most stable structures of NH_3*/$NH_{2(env)}$ on the Fe(111) surface at various corresponding coverages.

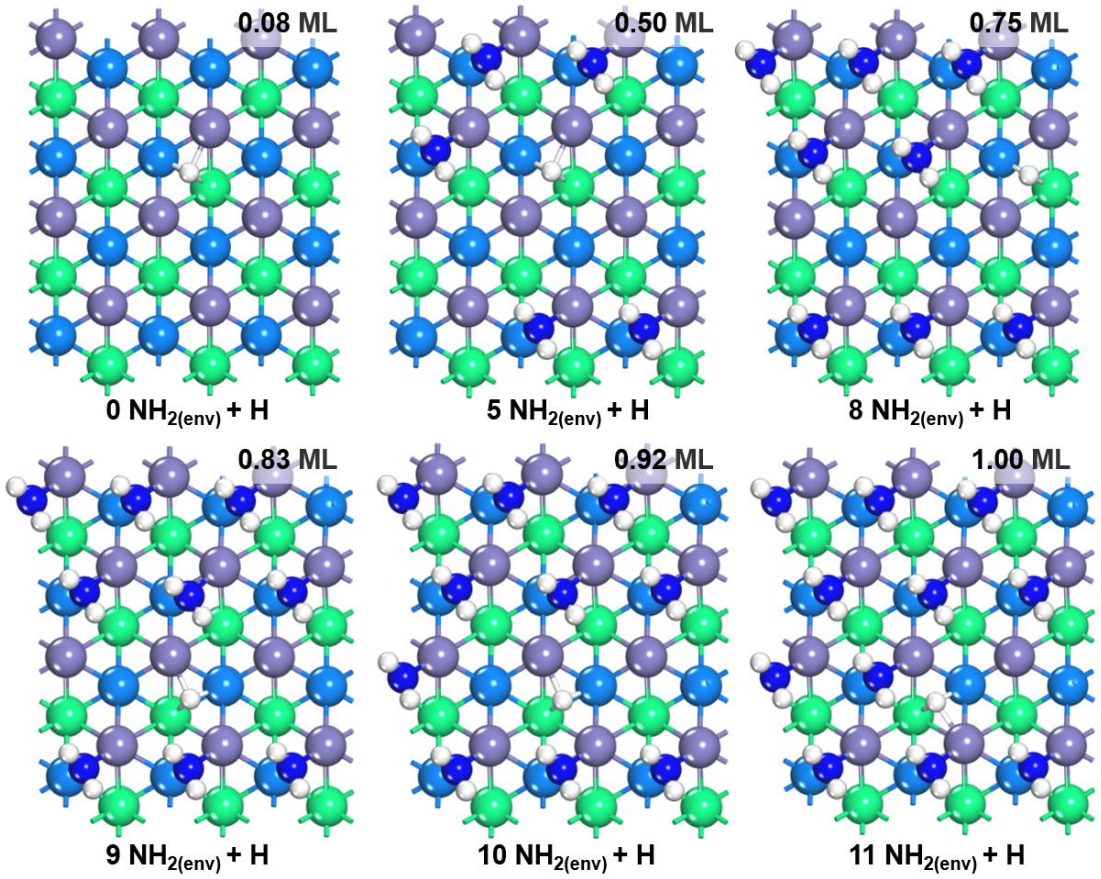

Fig. S9 Most stable structures of H*/$NH_{2(env)}$ on the Fe(111) surface at various corresponding coverages.

S4. Transition state structures of the coverage-dependent model

In this work, the coverage effects on the transition states of the rate-determining step (N-N-TS*) were rigorously calculated using the same method as one for the adsorption states. The most stable structure of transition state at each different coverage (0.17 to 1.00 ML) with different environment species (N, NH, NH_2, NH_3 and H) was searched, and an example set of structures of N-N-TS*/$NH_{2(env)}$ were shown in **Fig. S10**.

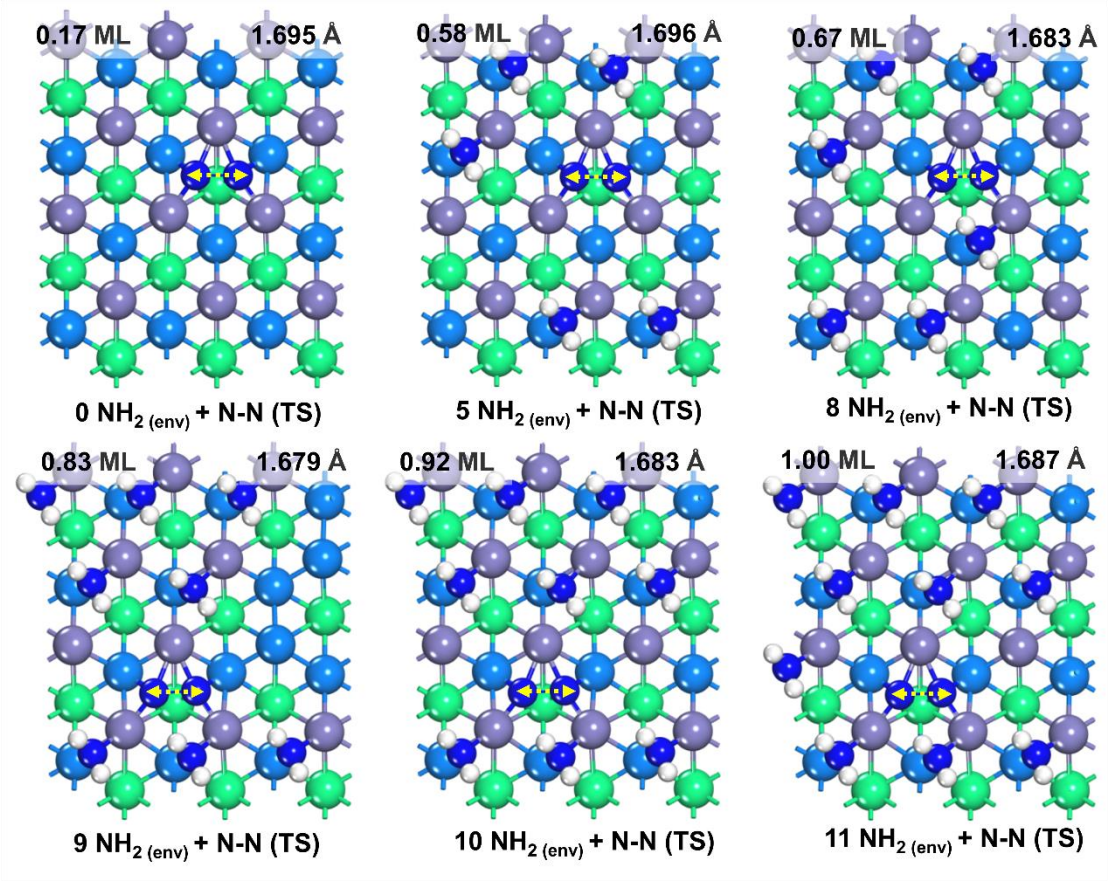

Fig. S10 Most stable structures of N-N(TS)*/$NH_{2(env)}$ on Fe(111) at various corresponding coverages.

S5. Descriptions of coverage effects

In this work, differential chemisorption energies were used in the kinetic simulations to account for the effects of both self- and cross-adsorbate-adsorbate interactions. As discussed before, optimized structures with different coverages on Fe(111) were calculated, and the differential chemisorption energies were represented by either two lines or one line (**Fig. S11-S15**). The coverage effects on the barriers of rate-determining step (N_2 dissociative adsorption barrier) are presented in **Fig. S16**.

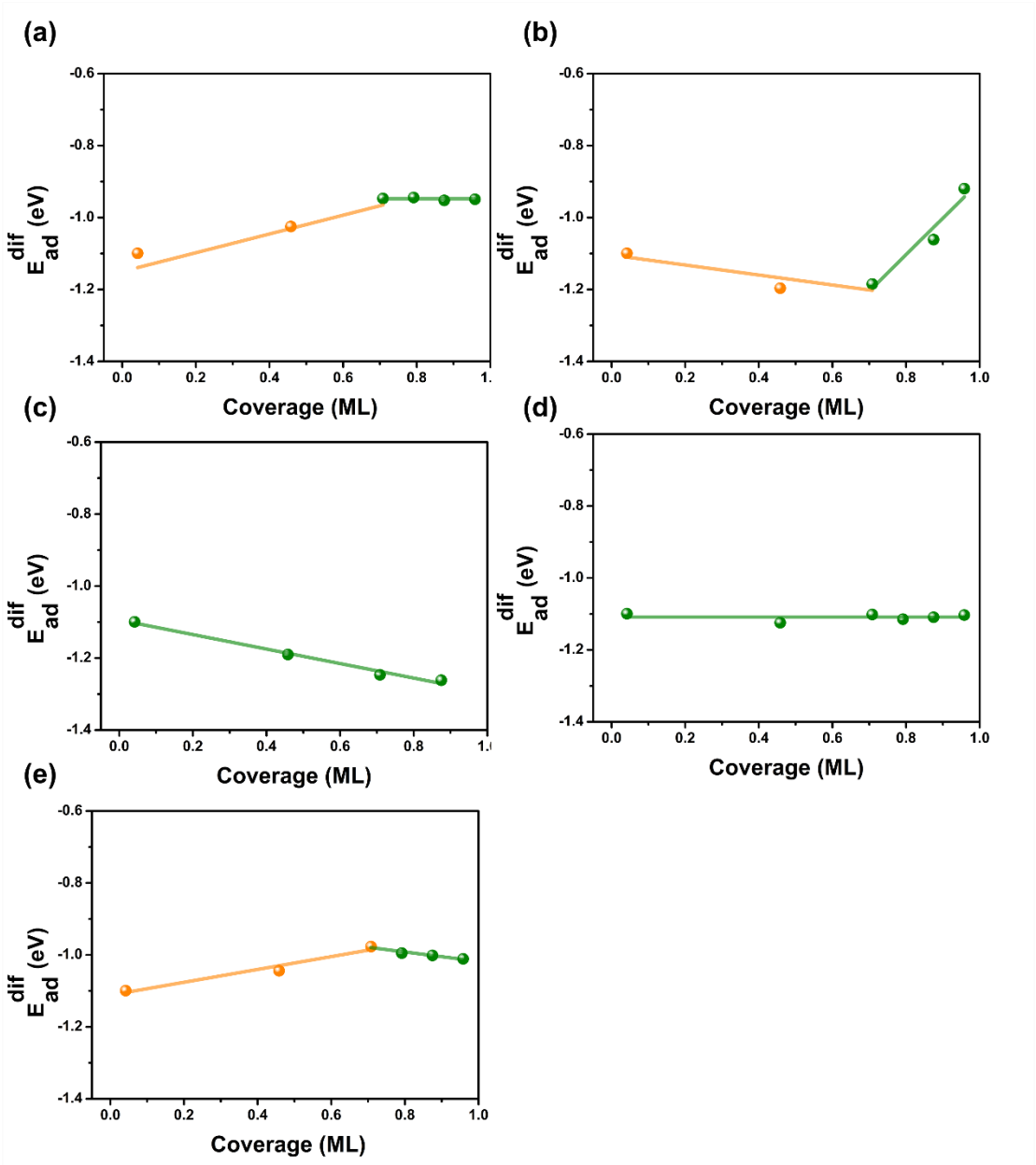

Fig. S11 Relationships between N differential adsorption energy and coverages of (a) N (defined as $N_{(env)}$ in the manuscript), (b) $NH_{2(env)}$, (c) $NH_{3(env)}$, (d) $H_{(env)}$ and (e) $NH_{(env)}$ on the p(3 × 3)-Fe(111) surface. The orange line represents the trend in the low coverage

range while the green line represents the trend in the high coverage range.

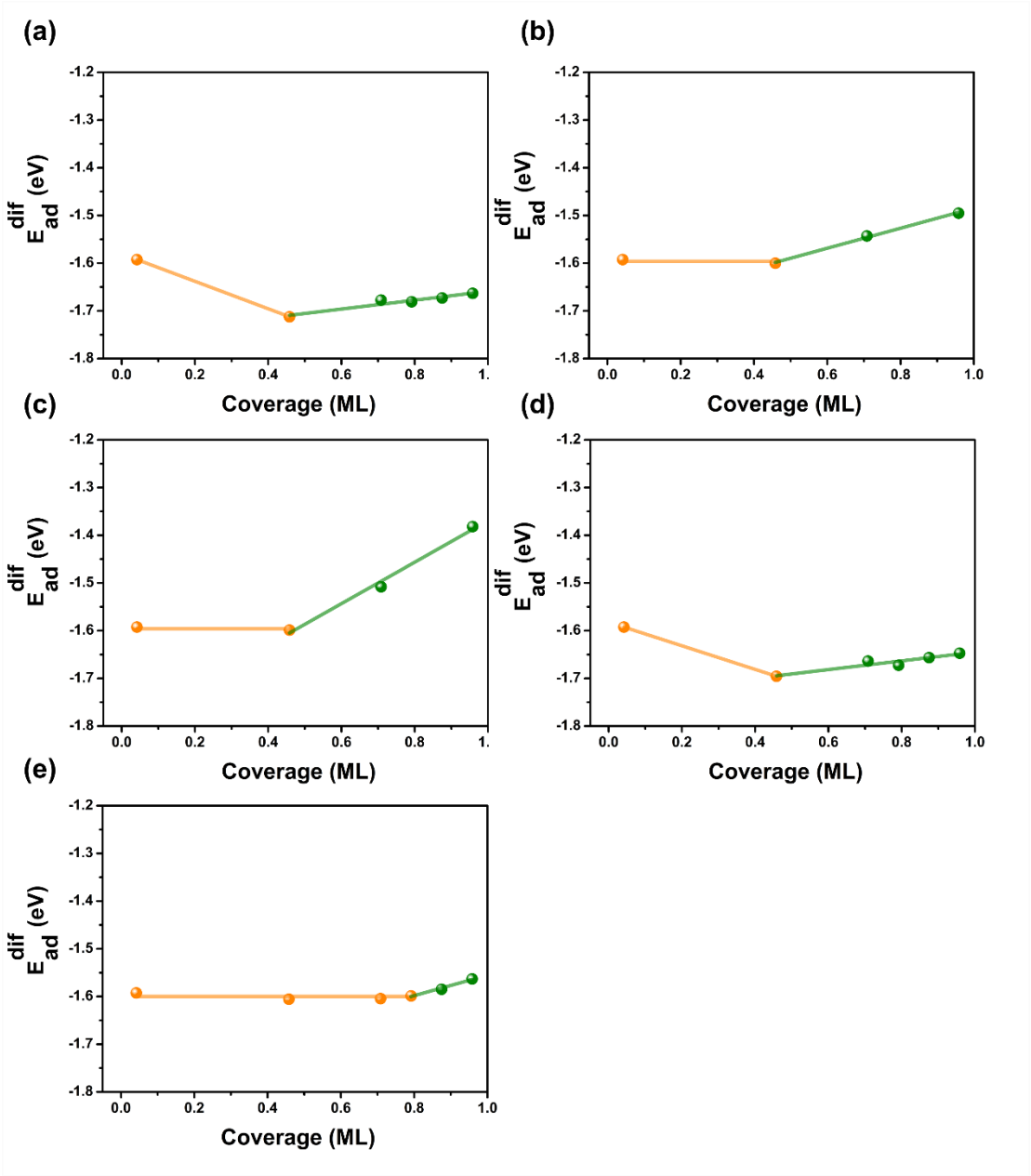

Fig. S12 Relationships between NH_2 differential adsorption energy and coverages of (a) $N_{(env)}$, (b) $NH_{2(env)}$, (c) $NH_{3(env)}$, (d) $H_{(env)}$ and (e) $NH_{(env)}$ on the p(3 × 3)-Fe(111) surface.

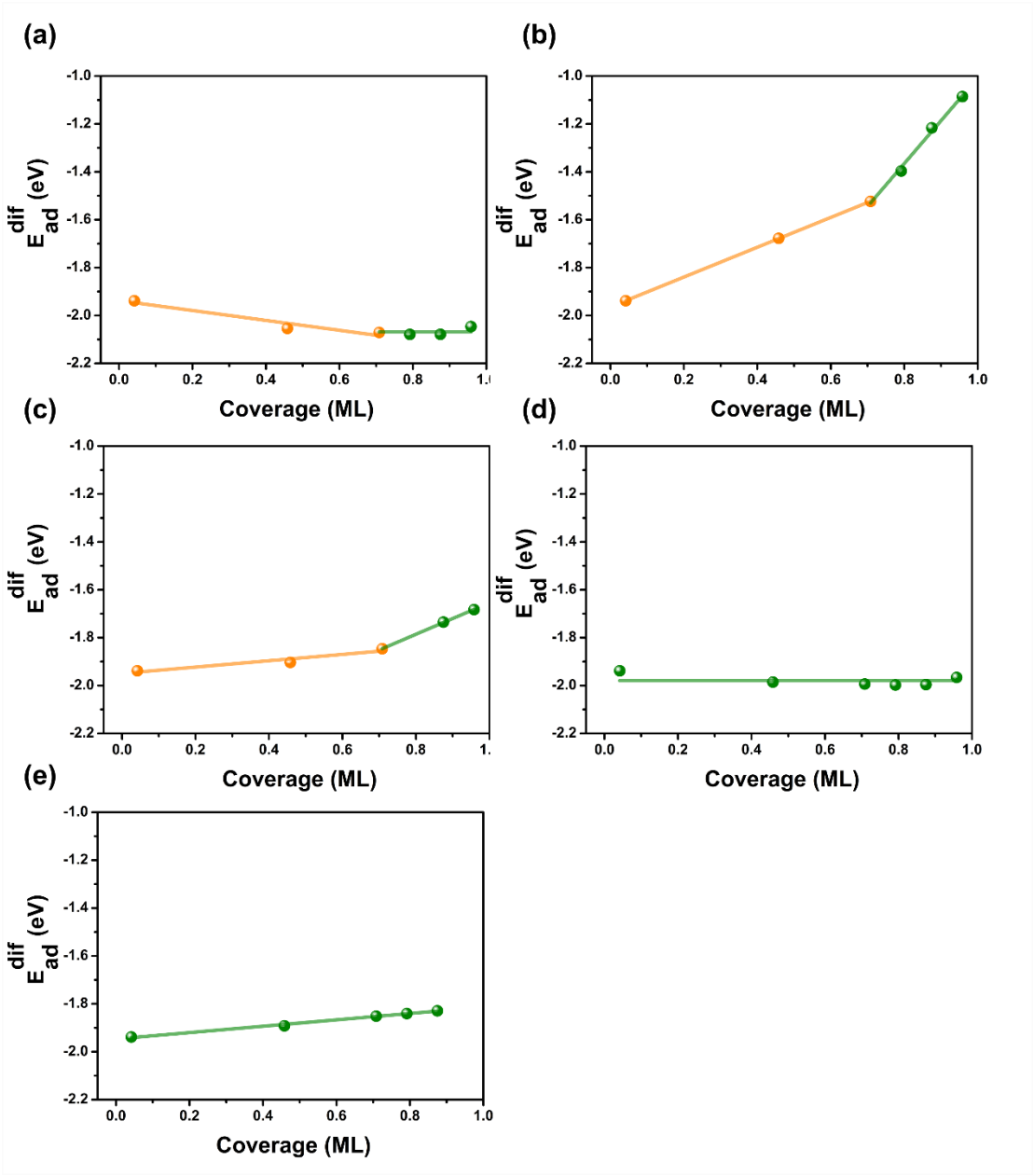

Fig. S13 Relationships between NH_3 differential adsorption energy and coverages of (a) $N_{(env)}$, (b) $NH_{2(env)}$, (c) $NH_{3(env)}$, (d) $H_{(env)}$ and (e) $NH_{(env)}$ on the p(3 × 3)-Fe(111) surface.

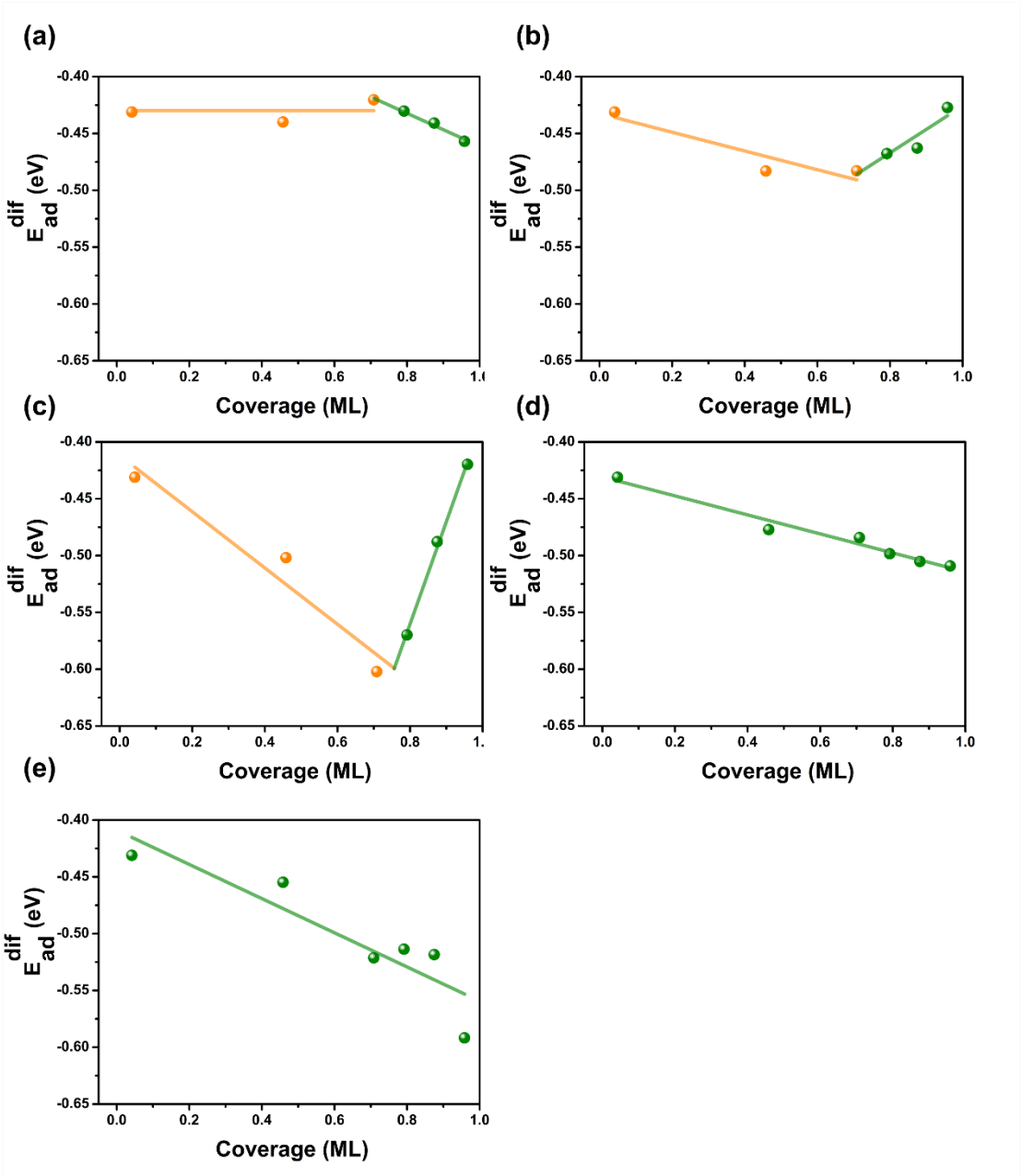

Fig. S14 Relationships between H differential adsorption energy and coverages of (a) $N_{(env)}$, (b) $NH_{2(env)}$, (c) $NH_{3(env)}$, (d) $H_{(env)}$ and (e) $NH_{(env)}$ on the p(3 × 3)-Fe(111) surface.

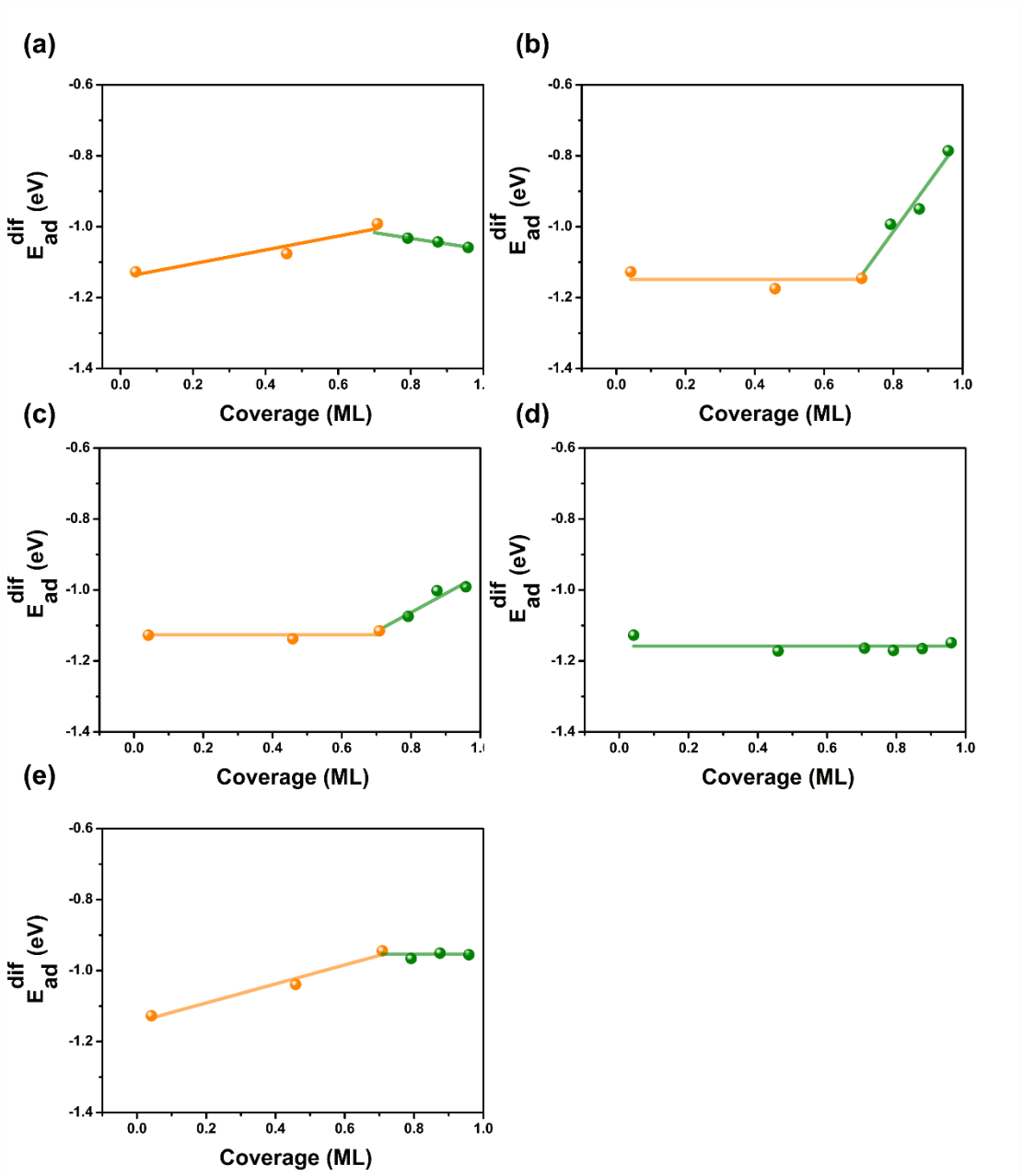

Fig. S15 Relationships between NH differential adsorption energy and coverages of (a) $N_{(env)}$, (b) $NH_{2(env)}$, (c) $NH_{3(env)}$, (d) $H_{(env)}$ and (e) $NH_{(env)}$ on the p(3 × 3)-Fe(111) surface.

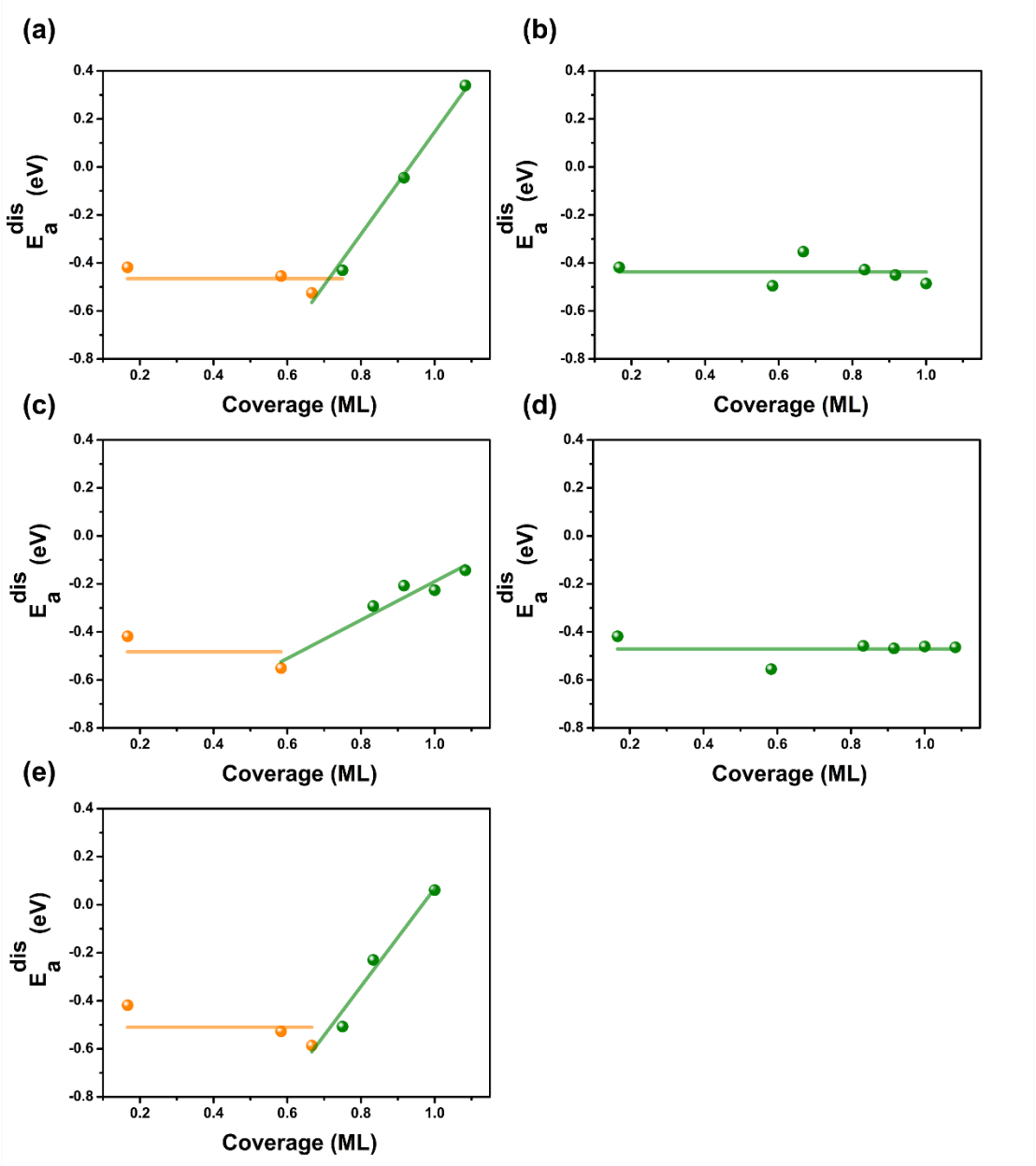

Fig. S16 Relationships between N_2 dissociative adsorption barrier and coverages of (a) $N_{(env)}$, (b) $NH_{2(env)}$, (c) $NH_{3(env)}$, (d) $H_{(env)}$ and (e) $NH_{(env)}$ on the p(3 × 3)-Fe(111) surface.

Table S3. List of slopes and intercepts of interaction curves between transition states of N_2 dissociative adsorption and adsorbates on *p*(3×3)-Fe(111). The interaction curves are shown in **Fig. S16**.

	low coverage		high coverage	
p(3 × 3)	slope	intercept	slope	intercept
N-N-TS*/$N_{(env)}$	0.000	-0.466	2.131	-1.985
N-N-TS*/$NH_{2(env)}$	0.000	-0.438	0.000	-0.438
N-N-TS*/$NH_{3(env)}$	0.000	-0.485	-0.801	-0.992
N-N-TS*/$H_{(env)}$	0.000	-0.471	0.000	-0.471
N-N-TS*/$NH_{(env)}$	0.000	-0.510	2.197	-2.118

S6. Thermodynamic corrections

All the energies used in the microkinetic modelling are free energies, corrected automatically in CATKINAS by considering the thermodynamic corrections of zero-point energy (ZPE), thermal energy (U), and entropy (S) derived from the vibrational partition function:

$$\Delta G_{ad}=E_{ad}+\Delta ZPE+\Delta U+RT-T\Delta S \quad \text{(S1)}$$

where E_{ad} is the total energy from VASP calculations. The zero-point energy correction was calculated as:

$$ZPE=\sum_i \frac{hv_i}{2} \quad \text{(S2)}$$

where h is Planck's constant and the vibrational frequencies v_i were calculated with one incoming adsorbate being relaxed while all the environmental adsorbates and the surface were fixed. The standard thermal energy contribution is calculated as:

$$U=RT\sum_i \frac{hv_i/K_B}{e^{hv_i/K_B T}-1} \quad \text{(S3)}$$

where R is the gas constant and K_B is the Boltzmann constant. The standard molar vibrational entropy is given by:

$$S=R\sum_i \left[\frac{hv_i/K_B}{e^{hv_i/K_B T}-1}-\ln(1-e^{-\frac{hv_i}{K_B T}})\right] \quad \text{(S4)}$$

For the adsorption or desorption processes, the accurate barriers of which are usually time-consuming to obtain by DFT calculations. Hence, we employed transition-state theory to estimate the adsorption or desorption energy barrier, where the entropy of gas is utilized.

S7. The self-consistent kinetics with coverage effect

The self-consistent kinetic calculations are illustrated in **Fig. S10**: An iterative approach with respect to the coverage is used and the convergence is controlled by monitoring the difference between the input coverage and the output coverage.

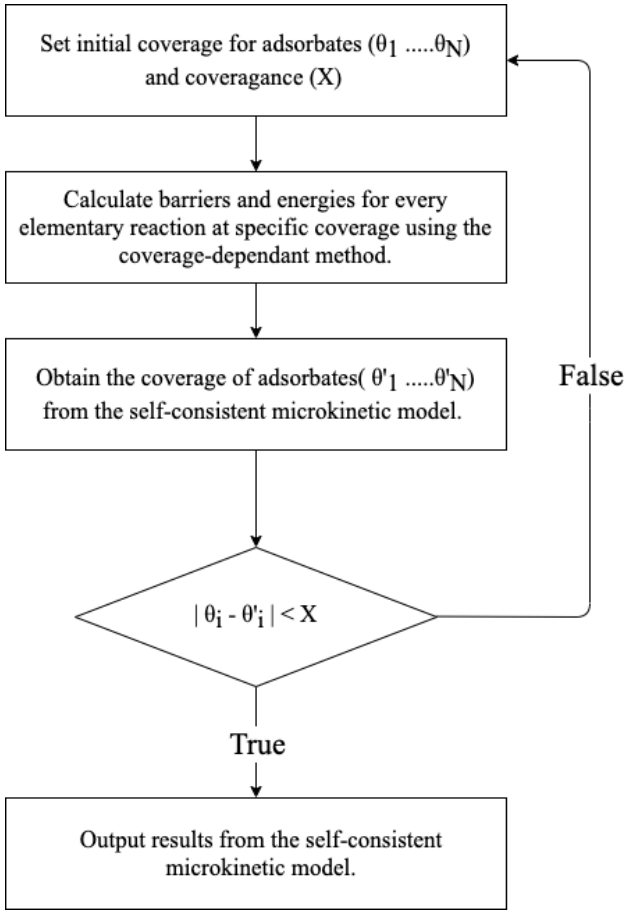

Fig. S17 Flow chart of the coverage-dependent microkinetic model, where X and θ represent the convergence and mixing weight of coverages, respectively.

S8. Applying the coverage effects on Fe(111) to other Fe surfaces

We utilized the coverage effects on the Fe(111) surface as approximate corrections for other Fe surfaces in order to streamline the computations. The corrected energy $E_i(\theta)$ was obtained from:

$$E_i(\theta) = E_{i0} + E_{correction} \quad \text{(S5)}$$

$$E_{correction}^{Fe(111)} = E_i^{Fe(111)}(\theta) - E_{i0}^{Fe(111)} \quad \text{(S6)}$$

$$E_i(\theta) = E_{i0} + E_i^{Fe(111)}(\theta) - E_{i0}^{Fe(111)} \quad \text{(S7)}$$

where E_{i0} is the original adsorption energy or reaction barrier from the low coverages on one certain Fe surface while $E_{correction}$ is the coverage correction term obtained through the two-line or one-line model.

The new activity, considering the coverage effects, was compared with the original activity at low coverages, as shown in **Table S4**.

Table S4. Activity (lg(TOF)) of various Fe surfaces with the coverage effects vs the one at low coverages. The reaction conditions are listed in the table.

lg(TOF)	coverage-independent		coverage-dependent
surface	673 K, 100 bar	673 K, 20 bar	673 K, 20 bar
Fe(110)	-9.94	-10.74	-12.35
Fe(100)	-9.05	-10.50	-12.29
Fe(210)	-4.80	-6.09	-6.07
Fe(211)	-3.70	-3.77	-2.10
Fe(111)	1.22	0.42	0.55

To further investigate the impact of the coverage effect, we have replotted the relationship between lg(TOF) and N_2 dissociative adsorption barrier, as illustrated in **Fig. S18(a)**. The distinction between stepped surfaces and flat surfaces becomes more apparent, and a better linear relationship with the N_2 dissociative adsorption barrier can be observed by referring to **Fig. 9(a)** for comparison. As anticipated, the surface energy continues to show a linear correlation with lg(TOF), as illustrated in **Fig. S18(b).**

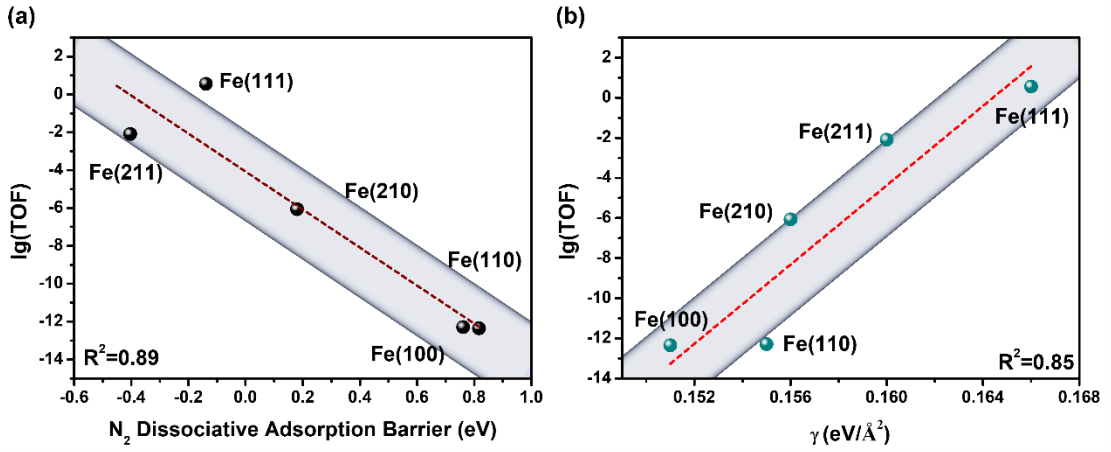

Fig. S18 Coverage-dependent microkinetic modelling results. **(**a) Relationship between lg(TOF) and N_2 dissociative adsorption barrier. (b) Relationship between lg(TOF) and surface energy.